Fractional Charge Density Functional Theory and Its Application to the Electro-Inductive Effect

Jun-Hyeong Kim[†,‡,∥], Dongju Kim[†,‡,∥], Weitao Yang[§,*], and Mu-Hyun Baik[‡,†,*]

[†]Department of Chemistry, Korea Advanced Institute of Science and Technology (KAIST), Daejeon 34141, Republic of Korea.

[‡]Center for Catalytic Hydrocarbon Functionalizations, Institute for Basic Science (IBS), Daejeon 34141, Republic of Korea.

[§]Department of Chemistry, Duke University, Durham, North Carolina 27708, United States

AUTHOR INFORMATION

Corresponding Author

*weitao.yang@duke.edu *mbaik2805@kaist.ac.kr

ABSTRACT

We employed the chemical potential neutralization principle to demonstrate that fractional electrons are involved in the electro-inductive effect as well as the vibrational Stark effect. By the chemical potential model, we were able to deduce that the frontier molecular orbitals of immobilized molecules can provide valuable insight into these effects. To further understand and

quantify these findings, we introduced fractional charge density functional theory (FC-DFT), a canonical ensemble approach for open systems. This method allows for the calculation of electronic energies, nuclear gradients, and the Hessian matrix of fractional electronic systems. To correct the spurious delocalization error commonly found in approximate density functionals for small systems, we imposed the Perdew-Parr-Levy-Balduz (PPLB) condition through linear interpolation of two adjacent integer points *(LI-FC-DFT)*. Although this approach is relatively simple in terms of molecular modeling, the results obtained through LI-FC-DFT calculations predict the same trend seen in experimental reactivity and the frequency change of immobilized molecules.

TOC GRAPHICS

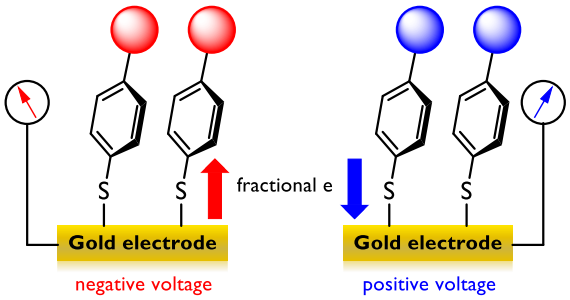

KEYWORDS Fractional Electrons, Density Functional Theory, Electro-inductive Effect, Vibrational Stark Effect, Grand-Canonical Ensemble

Manipulating the electronic properties of reactants through the use of functional groups is a key strategy for controlling chemical transformations and influencing the outcome of reactions. By understanding and controlling reaction barriers, chemists can accelerate the rate of desired reactions and suppress undesired pathways. For example, electron-donating groups can increase

electron density at the reaction center, lowering the barrier for a transition state that develops a positive partial charge. These effects have been quantified using the Hammett parameter, which measures the electron-donating and -withdrawing strengths of functional groups.[1] The use of functional groups has limitations, however, such as discontinuity in the Hammett parameters, side reactions, and the difficulty of synthesizing functionalized derivatives.

Recent developments have led to the emergence of a new approach that extends beyond the limitations of the traditional use of functional groups.[2-7] In 2020, two independent studies were reported by the Dawlaty and Baik groups, which provided proof-of-principle evidence for the possibility of using electrodes as functional groups with adjustable inductive effects. Target molecules were immobilized on a gold electrode, and voltage was applied in order to mimic the electron-donating and -withdrawing effects of traditional functional groups. The Baik group was able to control a variety of chemical reactions by adjusting the voltage on the electrode, and attributed this success to the "electro-inductive effect". In contrast, the Dawlaty group proposed that the observed changes in C–N vibrational frequency of aromatic nitriles immobilized on the surface were due to the vibrational Stark effect,[2] which is caused by the electric field generated by the applied voltage. In contrast, the Baumberg group posited that the changes in vibrational frequency were a result of ionic field effects,[8] wherein local electric fields created by electrolytes in the double layer alter the C–N frequency. Despite these competing proposals, the underlying mechanism of these effects remains elusive.

While the focus of the community has been on the electric field effects, we investigated whether the observed results can be attributed to electronic effects. In this paper, we propose a chemical potential model to demonstrate the role of fractional electrons in governing the observed

results, use frontier molecular orbitals to gain insight into the phenomenon, and present a computational protocol for modeling the electro-inductive effect in an efficient manner.

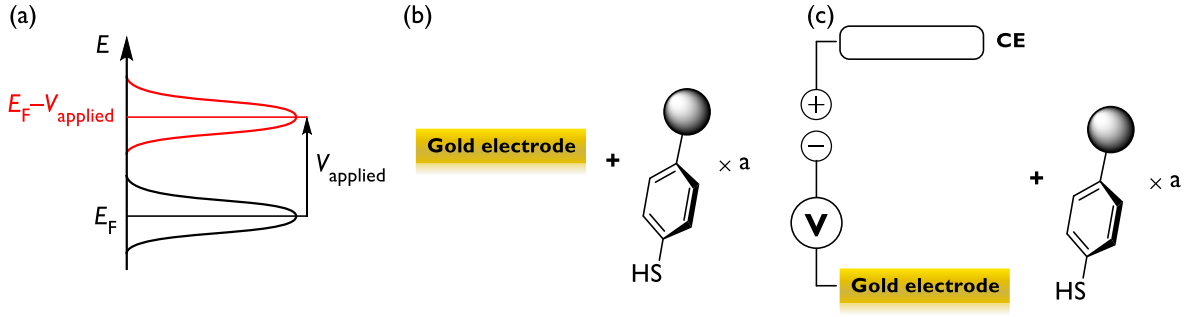

Figure 1. (a) Schematic illustration of the Fermi level before (black) and after (red) applying voltage. SAM formation between the gold electrode and 'a' number of molecules (b) without voltage and (c) with voltage.

Consider the reaction between the electrode and molecules that leads to the formation of a self-assembled monolayer (SAM). The application of voltage on the electrode changes the chemical potential neutralization condition[9-10] by shifting the Fermi level (Figure 1a). When no voltage is applied, the reaction proceeds until the chemical potential of the electrode ($\mu_{\text{electrode}}$) and 'a' number of molecules (μ_{mol}) are equal:

$$\mu_{electrode}(N_{electrode} + \Delta N) = \mu_{mol}(N_{mol} - \Delta N/a) \quad (1)$$

, where ΔN indicates the number of electrons involved in the reaction. The expression ΔN can be obtained by taking the Taylor expansion up to the first order, considering that the absolute hardness (η) of conductors is zero:[10]

$$\frac{\Delta N}{a} = \frac{\mu_{mol}(N_{mol}) - \mu_{electrode}(N_{electrode})}{2\eta_{mol}} \quad (2)$$

In contrast, applying voltage ($V_{applied}$) on the electrode changes the condition by shifting the Fermi level (Figure 1c):

$$\mu_{\text{electrode}}\left(N_{electrode}+\Delta N+\alpha\left(V_{applied}\right)\right)-V_{applied}=\mu_{mol}\left(N_{mol}-\frac{\Delta N+\alpha(V_{applied})}{a}\right) \quad (3)$$

Note that the application of voltage leads to an additional charge transfer, denoted as $\alpha(V_{applied})$, during the formation of the SAM. This additional charge transfer can be represented by the change in the number of electrons of the immobilized molecule, which can be further represented by the density change of the molecule ($\Delta\rho_{mol}(\mathbf{r})$):

$$\delta\rho_{\text{mol}}(\boldsymbol{r})=\frac{\partial\rho_{mol}(\boldsymbol{r})}{\partial N}\cdot\frac{\partial N}{\partial V_{applied}}\cdot\delta V_{applied}$$

$$=f_{mol}(\boldsymbol{r})\cdot\frac{\partial N}{\partial\mu}\cdot\delta V_{applied}$$

$$=S_{mol}f_{mol}(\boldsymbol{r})\delta V_{applied} \quad (4)$$

, where S_{mol} and $f_{mol}(\mathbf{r})$ indicate absolute softness and the Fukui function of the immobilized molecule.[9, 11] Thus, the final equation reads:

$$\Delta\rho_{\text{mol}}(\boldsymbol{r})=S_{mol}f_{mol}(\boldsymbol{r})V_{applied} \quad (5)$$

We have derived an expression for $\Delta\rho_{mol}(\mathbf{r})$ resulting from $V_{applied}$. It is important that $\Delta\rho_{mol}(\mathbf{r})$ does not necessarily correspond to integer numbers, allowing for fractional electrons that move back and forth in response to changes in the applied voltage. This feature makes density functional theory (DFT) the method of choice for implementing this model into a quantum chemical framework, as fractional charges and non-integer electron densities are well-defined in DFT.[12] Furthermore, our derivation revealed that $\Delta\rho_{mol}(\mathbf{r})$ is directly related to the Fukui

function,[11] which implies that the experimental observations can be qualitatively understood by the frontier molecular orbitals of the immobilized molecule.

Next, we sought to create a quantitative model that incorporated eq. 5 and explicitly considers the presence of fractional, non-integer number of electrons in the molecule. Although the concept of non-integer numbered density for molecules has a long history in DFT,[12-16] we are using it here to establish a connection to the chemical reactivity of such a species. Previously, the Arias and Hammes-Schiffer groups presented a model considering the electric field associated with the applied voltage.[4, 17-20] The Arias group adopted a grand-canonical approach in conjunction with joint density functional theory,[17-19] and developed an algorithm for the self-consistent field method (GC-AuxH) by varying the number of fractional electrons under fixed chemical potential.[20] While the GC-AuxH algorithm achieved robust convergence that has remained a main challenge in fixed-potential GC-DFT, it is not suitable for our purposes as the structure is only obtained at $V_{applied} = 0$ due to the lack of analytical nuclear gradients at a given voltage. In contrast, the Hammes-Schiffer group utilized a canonical ensemble approach by incorporating fractional electrons (fixed-electron) to the system directly and tried to explain Dawlaty's work with a discontinuous dielectric constant of the solvent, which is consistent with the Gouy-Chapman-Stern model.[4] This approach ensures more robust convergence compared to fixed-potential calculations and enables the optimization of the structure with various number of fractional electrons, but it can suffer from severe delocalization errors caused by these fractional electrons.[13-14, 21] In addition, the complex experimental condition, the electrode surface and the interface for example, makes detailed simulations of electrode-molecule systems challenging to coin the atomic details.

Inspired by the chemical potential model and previous works mentioned above, we propose the fractional charge DFT (FC-DFT) as a canonical ensemble approach for describing the electro-

inductive effect. In FC-DFT, we use a fixed electron number to determine the properties of the system based on the fractional charge total energy $E(N+\delta)$ and the associated electron density. Unlike the fixed-potential approach in a grand canonical ensemble (GC-DFT), FC-DFT calculates the system properties at a fixed average electron number. Electric fields generated by the applied voltage can also be included in the FC-DFT through an external potential. While GC-DFT and FC-DFT should be equivalent, in principle, FC-DFT has several potential advantages over GC-DFT: 1) FC-DFT allows for effective modeling of the electro-inductive effect with a much smaller model system than the much larger system of combined molecule and electrode, which is necessary in the GC-DFT approach. 2) FC-DFT leads to a much more efficient approach to self-consistent calculations required in DFT energy minimization due to the use of fixed electron numbers. 3) For small model systems, FC-DFT can easily bypass the delocalization error commonly encountered in density functional approximations (DFAs).

In our initial implementation, we focused on a small model system and ignored the direct electric field effects. We neglect the field effects because of the assumption that the field is screened by the metallic electrodes and the solvents, as mentioned above. The next challenge is associated with the delocalization error in DFAs,[13-14, 21] which can lead to a large systematic error in the energy $E(N+\delta)$ and charge density for fractional number of electrons. Fortunately, for systems small in terms of the number of atoms and physical extent, the total energies for integer numbers of electrons are typically accurate,[21-22] and we can thus utilize the exact Perdew-Parr-Levy-Balduz (PPLB) condition[12] for calculating systems with fractional electrons, namely

$$E(N+\delta) = (1-\delta)E(N) + \delta E(N+1) \quad (6)$$

Commonly used DFA suffer from the delocalization error, where $E(N+\delta) < (1-\delta)E(N) + \delta E(N+1)$ breaks the linearity of E *vs.* δ and gives a convex curve.[21] Given the size of 4-mercaptobenzonitrile

(MBN) and *tert*-butyl-4-mercaptobenzoate (TBMB), DFAs may produce reasonable results on integer points of these molecules. Therefore, we decided to take a linear interpolation approach when evaluating $E(N+\delta)$. This method, which involves interpolating between two adjacent integer points at $N+\delta$, is referred to as linear interpolation FC-DFT (LI-FC-DFT). With LI-FC-DFT, we will perform geometry optimization utilizing the nuclear gradient $\mathbf{g}(N+\delta)$ (eq. 7), and subsequently diagonalize the Hessian matrix $\mathbf{H}(N+\delta)$ derived from the optimized structure as outlined in eq. 8.

$$\boldsymbol{g}(N+\delta) = (1-\delta)\boldsymbol{g}(N) + \delta\boldsymbol{g}(N+1) \quad (7)$$

$$\boldsymbol{H}(N+\delta) = (1-\delta)\boldsymbol{H}(N) + \delta\boldsymbol{H}(N+1) \quad (8)$$

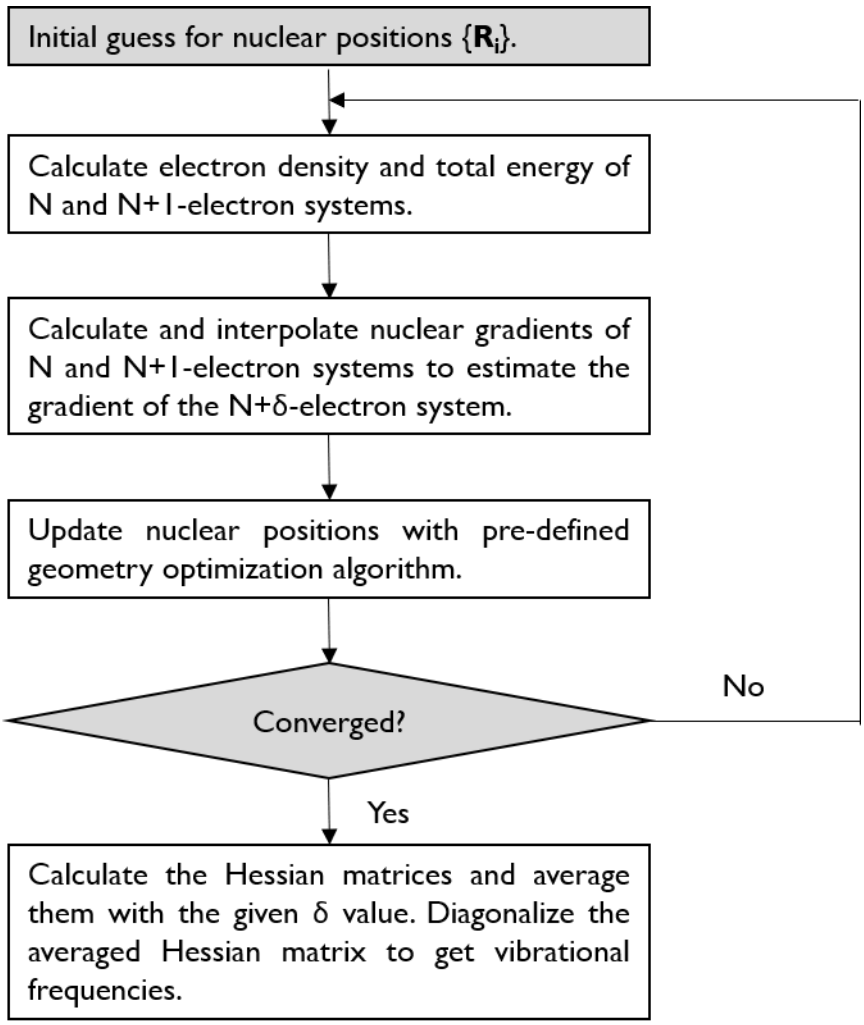

Figure 2. Workflow of the LI-FC-DFT.

Figure 2 summarizes the algorithm of LI-FC-DFT calculations. The algorithm is similar to that of conventional geometry optimization except for performing two separate SCF cycles in each geometry iteration to calculate $E(N+\delta)$ and $\mathbf{g}(N+\delta)$. Once a stationary point is located, $\mathbf{H}(N)$ and $\mathbf{H}(N+1)$ of the optimized structure are computed to obtain $\mathbf{H}(N+\delta)$, which is then diagonalized to estimate vibrational frequencies required for evaluating zero-point energies and the vibrational partition function. The LI-FC-DFT algorithm was implemented with python-based geomeTRIC,[23] which is an open-source geometry optimizer, and all DFT calculations[16, 24-25] were carried out as implemented in Jaguar 9.1.[26] For estimating the reaction barrier, the energies of the optimized structures were re-evaluated by additional single-point calculations on each optimized geometry with Dunning's correlation consistent triple-ζ basis set cc-pVTZ(-f),[27] which includes a double set of polarization functions. Solvation energies were evaluated by a self-consistent reaction field (SCRF) approach based on accurate numerical solutions of the Poisson-Boltzmann equation. In the results reported below, solvation calculations were carried out with the 6-31G** basis[28] at the optimized gas-phase geometry employing the dielectric constants of ε = 78.4 for water. As is the case for all continuum models, the solvation energies are subject to empirical parametrization of the atomic radii that are used to generate the solute surface. We employed the standard set of optimized radii in Jaguar for H (1.150 Å), C (1.900 Å), O (1.600 Å), and S (1.900 Å). Analytical vibrational frequencies within the harmonic approximation were computed with the 6-31G** basis to confirm proper convergence to well-defined minima or saddle points on the potential energy surface. The energy components have been computed with the following protocol. The free energy in solution-phase, $G(\text{sol})$ has been calculated as follows:

$$G(\text{sol}) = G(\text{gas}) + G_{\text{solv}} \quad (9)$$

$$G(\text{gas}) = H(\text{gas}) - TS(\text{gas}) \quad (10)$$

$$H(\text{gas}) = E(\text{SCF}) + \text{ZPE} \quad (11)$$

$$\Delta E(\text{SCF}) = \Sigma\, E(\text{SCF}) \text{ for products} - \Sigma\, E(\text{SCF}) \text{ for reactants} \quad (12)$$

$$\Delta G(\text{sol}) = \Sigma\, G(\text{sol}) \text{ for products} - \Sigma\, G(\text{sol}) \text{ for reactants} \quad (13)$$

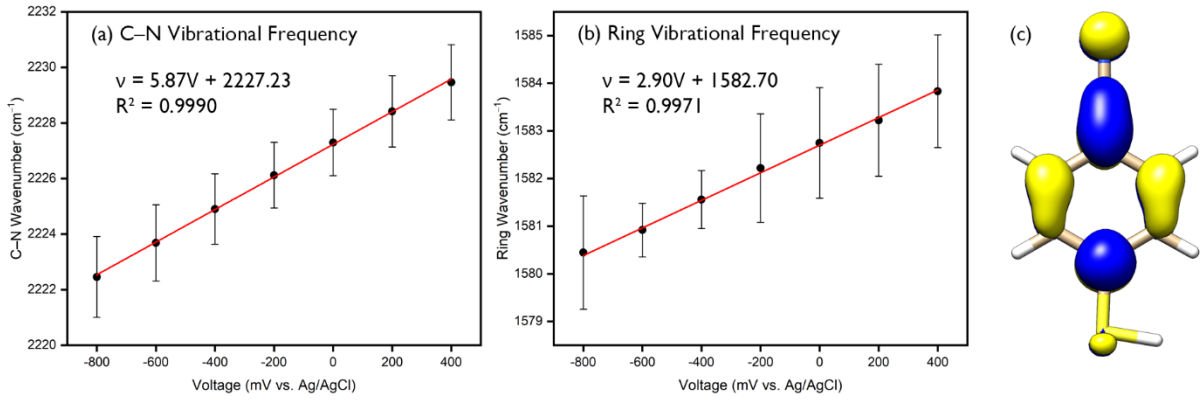

Figure 3. Voltage-dependent surface-enhanced Raman spectroscopy (SERS) spectra of 4-mercaptobenzonitrile immobilized on the gold electrode. The SERS spectra were obtained with excitation wavelength of 633 nm under in situ electrochemical conditions at 7 different voltages (*vs.* Ag/AgCl). 1 M KCl in deionized water is used as the electrolyte solution. The Au plate decorated with SAM was utilized as the working electrode, and the Pt wire served as the counter electrode. The vibrational frequency of each mode was extracted by performing a Gaussian fit on the spectra. See the Supporting Information for the experimental details. (a) C–N vibrational frequency and (b) ring vibrational frequency. (c) DFT-calculated LUMO of 4-mercaptobenzonitrile (isovalue = 0.05 e/Å^3) at CAM-B3LYP/6-31+G** level of theory.[28-29]

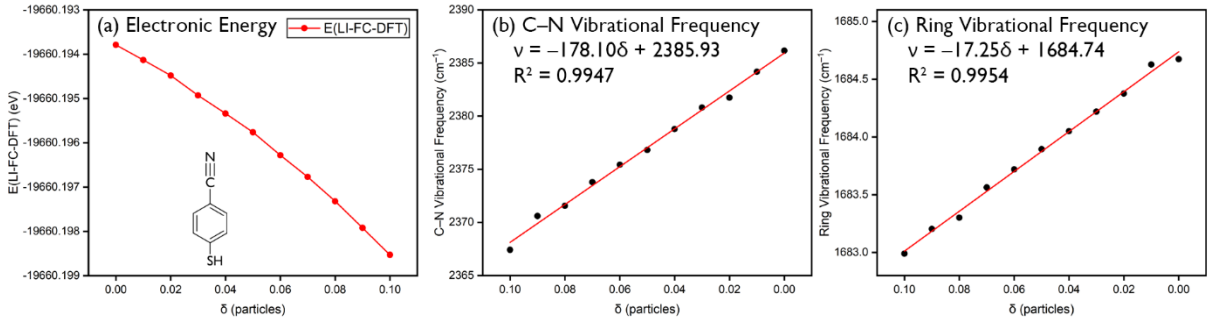

Figure 4. LI-FC-DFT-calculated (a) electronic energy, (b) C–N vibrational frequency, and (c) ring vibrational frequency of 4-mercaptobenzonitrile at CAM-B3LYP/6-31+G** level of theory.[28-29] Note that the x-axis (δ) of (b) and (c) is intentionally reversed to be consistent with experimental data.

Figure 4 illustrates the LI-FC-DFT-calculated results for the MBN molecule. To ensure a bound state, a range-separated functional and diffuse functions were incorporated in the modeling to avoid the presence of unbound electrons caused by a negatively charged molecule. (Figure 4a). The calculated C–N stretching and ring vibrational frequencies (Figure 4b and 4c, respectively) show a trend that is in good agreement with the experimental observations,[2, 8] as depicted in Figure 3a and 3b, respectively. The LI-FC-DFT calculations predict that these frequencies will become blue-shifted as fractional electrons are removed from the MBN molecule starting from a state with a partial occupied LUMO. This behavior can be explained by the fractional occupation of the frontier molecular orbitals (eq. 5). We estimated that, using eq. 2, the LUMO (Figure 3c), which has both C–N antibonding character and two nodes on the ring fragment, is already partially occupied by 0.131 electrons during the SAM formation (Table S1) at the absolute zero voltage. As the positive voltage is applied, more fractional electrons are taken away from this partially occupied orbital, which strengthens the C–N bond. Similarly, the shift in the ring vibrational

frequency can be attributed to the same fractional removal of electron density from this MO, which possesses ring antibonding character as illustrated by the presence of two nodes.

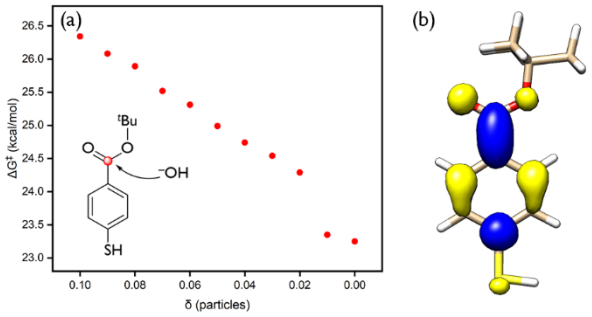

Figure 5. (a) LI-FC-DFT-calculated reaction barriers of the base-catalyzed hydrolysis of *tert*-butyl-4-mercaptobenzoate at B3LYP-D3/cc-pVTZ(-f)//6-31G** (SCRF, ε = 78.4 for water) level of theory.[27, 30-37] Note that the x-axis (δ) is intentionally reversed to be consistent with experimental data. (b) DFT-calculated LUMO of *tert*-butyl-4-mercaptobenzoate (isovalue = 0.05 e/Å^3) at B3LYP-D3/6-31G** level of theory.

Encouraged by the matching shift of vibrational frequencies, we modeled the base-catalyzed ester hydrolysis reaction to confirm that the application of positive voltage increases the reaction rate. Previous study by Wang indicates that the nucleophilic attack by the hydroxide ion is rate-determining.[38] Thus, we located the transition state where the hydroxide ion attacks the ester moiety of TBMB, and the calculated results are illustrated in Figure 5. Unlike what was described above, diffuse functions were excluded in the basis set and a hybrid functional was employed to accelerate the calculations. Except for the discontinuity at $\delta = 0.02$ caused by the thiol rotation, the calculated reaction barrier smoothly decreases as more fractional electrons are taken away from TBMB, which is consistent with the experimental observation that positive voltage

accelerates the reaction.[3] The decrease in the barrier can be rationalized with the fractional occupation of what is the LUMO of free TBMB. Before applying a voltage, this MO already acquires 0.072 electrons from the electrode during the SAM formation (Table S2), and this orbital plays a crucial role in promoting the nucleophilic attack by the hydroxide ion. Thus, in terms of Fukui functions, this partially occupied MO still acts mostly as the LUMO of the molecule. As it gains more fractional electrons, the reaction rate decreases as the LUMO is unable to moderate the interaction with the incoming nucleophile. In other words, the fractionally occupied MO loses LUMO character and increasingly gains HOMO character. As this process continues with higher negative voltage, the higher-lying LUMO+1 becomes fractionally occupied, which raises the transition state energy.

In summary, our study reveals that the change in both vibrational frequencies and reaction barriers constituting the electro-inductive effect can be understood by fractional electrons in the frontier molecular orbitals without explicitly considering the electric field effects. Our findings were supported by the use of LI-FC-DFT, which represents the initial implementation of FC-DFT. Throughout the detailed analysis, we found the presence of electronic effects that is distinctively different from the vibrational Stark effect. While LI-FC-DFT has produced satisfactory results for small systems, its application to larger systems is currently limited as the E vs. N curve becomes linear independent of the delocalization error in the functionals and the energies for the charged systems with integer number of electrons having systematic delocalization error. Therefore, for large systems, it necessitates developing a general and more robust implementation of FC-DFT with the application of the localized orbital scaling corrections, for example.[39-41] Additionally, calibration of the calculated results with experiments, *i.e.* how many fractional electrons

correspond to the experimentally applied voltage, is necessary in order to make FC-DFT a more precise and predictive tool. These studies are ongoing in our laboratories.

ASSOCIATED CONTENT

Supporting Information. The Supporting Information is available free of charge at https://pubs.acs.org/. Experimental details, LI-FC-DFT-computed energy components and energy derivatives, Cartesian coordinates and vibrational frequencies of all computed structures (PDF)

Code Availability

The LI-FC-DFT code is available at https://github.com/JunHyeong1/LI-FC-DFT/tree/master.

AUTHOR INFORMATION

ORCID

Jun-Hyeong Kim: 0000-0001-7747-5475

Dongju Kim: 0000-0001-6334-1572

Weitao Yang: 0000-0001-5576-2828

Mu-Hyun Baik: 0000-0002-8832-8187

Notes

[‖]These authors equally contributed to the work.

ACKNOWLEDGMENT

We thank the Institute for Basic Science in Korea for financial support (IBS-R10-A1) and the National Science Foundation (grant no. CHE-1900338). Text in the introduction section was improved for grammar and style of presentation by using ChatGPT.

REFERENCES

1. Hammett, L. P., The Effect of Structure upon the Reactions of Organic Compounds. Benzene Derivatives. *J. Am. Chem. Soc.* **1937,** *59*, 96-103.
2. Sarkar, S.; Patrow, J. G.; Voegtle, M. J.; Pennathur, A. K.; Dawlaty, J. M., Electrodes as Polarizing Functional Groups: Correlation between Hammett Parameters and Electrochemical Polarization. *J. Phys. Chem. C* **2019,** *123*, 4926-4937.
3. Heo, J.; Ahn, H.; Won, J.; Son, J. G.; Shon, H. K.; Lee, T. G.; Han, S. W.; Baik, M.-H., Electro-Inductive Effect: Electrodes as Functional Groups with Tunable Electronic Properties. *Science* **2020,** *370*, 214-219.
4. Goldsmith, Z. K.; Secor, M.; Hammes-Schiffer, S., Inhomogeneity of Interfacial Electric Fields at Vibrational Probes on Electrode Surfaces. *ACS Cent Sci* **2020,** *6*, 304-311.
5. Delley, M. F.; Nichols, E. M.; Mayer, J. M., Interfacial Acid-Base Equilibria and Electric Fields Concurrently Probed by *In Situ* Surface-Enhanced Infrared Spectroscopy. *J. Am. Chem. Soc.* **2021,** *143*, 10778-10792.
6. Sarkar, S.; Maitra, A.; Lake, W. R.; Warburton, R. E.; Hammes-Schiffer, S.; Dawlaty, J. M., Mechanistic Insights about Electrochemical Proton-Coupled Electron Transfer Derived from a Vibrational Probe. *J. Am. Chem. Soc.* **2021,** *143*, 8381-8390.
7. Hammes-Schiffer, S.; Galli, G., Integration of Theory and Experiment in the Modelling of Heterogeneous Electrocatalysis. *Nature Energy* **2021,** *6*, 700-705.
8. Wright, D.; Sangtarash, S.; Mueller, N. S.; Lin, Q.; Sadeghi, H.; Baumberg, J. J., Vibrational Stark Effects: Ionic Influence on Local Fields. *J. Phys. Chem. Lett.* **2022,** *13*, 4905-4911.
9. Parr, R. G.; Pearson, R. G., Absolute Hardness: Companion Parameter to Absolute Electronegativity. *J. Am. Chem. Soc.* **1983,** *105*, 7512-7516.
10. Pearson, R. G., *Chemical Hardness: Applications from Molecules to Solids*. Wiley-VCH Verlag: Weinheim, Germany, 1997.
11. Parr, R. G.; Yang, W., Density Functional Approach to the Frontier-Electron Theory of Chemical Reactivity. *J. Am. Chem. Soc.* **1984,** *106*, 4049-4050.
12. Perdew, J. P.; Parr, R. G.; Levy, M.; Balduz, J. L., Density-Functional Theory for Fractional Particle Number: Derivative Discontinuities of the Energy. *Phys. Rev. Lett.* **1982,** *49*, 1691-1694.
13. Cohen, A. J.; Mori-Sánchez, P.; Yang, W., Insights into Current Limitations of Density Functional Theory. *Science* **2008,** *321*, 792-794.
14. Cohen, A. J.; Mori-Sánchez, P.; Yang, W., Challenges for Density Functional Theory. *Chem. Rev.* **2012,** *112*, 289-320.
15. Teale, A. M.; Helgaker, T.; Savin, A.; Adamo, C.; Aradi, B.; Arbuznikov, A. V.; Ayers, P. W.; Baerends, E. J.; Barone, V.; Calaminici, P.; Cancès, E.; Carter, E. A.; Chattaraj, P. K.; Chermette, H.; Ciofini, I.; Crawford, T. D.; De Proft, F.; Dobson, J. F.; Draxl, C.; Frauenheim, T.; Fromager, E.; Fuentealba, P.; Gagliardi, L.; Galli, G.; Gao, J.; Geerlings, P.; Gidopoulos, N.;

Gill, P. M. W.; Gori-Giorgi, P.; Görling, A.; Gould, T.; Grimme, S.; Gritsenko, O.; Jensen, H. J. A.; Johnson, E. R.; Jones, R. O.; Kaupp, M.; Köster, A. M.; Kronik, L.; Krylov, A. I.; Kvaal, S.; Laestadius, A.; Levy, M.; Lewin, M.; Liu, S.; Loos, P.-F.; Maitra, N. T.; Neese, F.; Perdew, J. P.; Pernal, K.; Pernot, P.; Piecuch, P.; Rebolini, E.; Reining, L.; Romaniello, P.; Ruzsinszky, A.; Salahub, D. R.; Scheffler, M.; Schwerdtfeger, P.; Staroverov, V. N.; Sun, J.; Tellgren, E.; Tozer, D. J.; Trickey, S. B.; Ullrich, C. A.; Vela, A.; Vignale, G.; Wesolowski, T. A.; Xu, X.; Yang, W., DFT Exchange: Sharing Perspectives on the Workhorse of Quantum Chemistry and Materials Science. *Phys. Chem. Chem. Phys.* **2022,** *24*, 28700-28781.
16. Parr, R. G.; Weitao, Y., *Density-Functional Theory of Atoms and Molecules*. Oxford University Press: 1994.
17. Petrosyan, S. A.; Rigos, A. A.; Arias, T. A., Joint Density-Functional Theory: Ab Initio Study of Cr_2O_3 Surface Chemistry in Solution. *J. Phys. Chem. B* **2005,** *109*, 15436-15444.
18. Petrosyan, S. A.; Briere, J.-F.; Roundy, D.; Arias, T. A., Joint Density-Functional Theory for Electronic Structure of Solvated Systems. *Phys. Rev. B* **2007,** *75*, 205105.
19. Letchworth-Weaver, K.; Arias, T. A., Joint Density Functional Theory of the Electrode-Electrolyte Interface: Application to Fixed Electrode Potentials, Interfacial Capacitances, and Potentials of Zero Charge. *Phys. Rev. B* **2012,** *86*, 075140.
20. Sundararaman, R.; Goddard, W. A., III; Arias, T. A., Grand Canonical Electronic Density-Functional Theory: Algorithms and Applications to Electrochemistry. *J. Chem. Phys.* **2017,** *146*, 114104.
21. Mori-Sánchez, P.; Cohen, A. J.; Yang, W., Localization and Delocalization Errors in Density Functional Theory and Implications for Band-Gap Prediction. *Phys. Rev. Lett.* **2008,** *100*, 146401.
22. Mei, Y.; Chen, Z.; Yang, W., Exact Second-Order Corrections and Accurate Quasiparticle Energy Calculations in Density Functional Theory. *J. Phys. Chem. Lett.* **2021,** *12*, 7236-7244.
23. Wang, L.-P.; Song, C., Geometry Optimization Made Simple with Translation and Rotation Coordinates. *J. Chem. Phys.* **2016,** *144*, 214108.
24. Hohenberg, P.; Kohn, W., Inhomogeneous Electron Gas. *Phys. Rev.* **1964,** *136*, B864-B871.
25. Kohn, W.; Sham, L. J., Self-Consistent Equations Including Exchange and Correlation Effects. *Phys. Rev.* **1965,** *140*, A1133-A1138.
26. Bochevarov, A. D.; Harder, E.; Hughes, T. F.; Greenwood, J. R.; Braden, D. A.; Philipp, D. M.; Rinaldo, D.; Halls, M. D.; Zhang, J.; Friesner, R. A., Jaguar: A High-Performance Quantum Chemistry Software Program with Strengths in Life and Materials Sciences. *Int. J. Quantum Chem.* **2013,** *113*, 2110-2142.
27. Dunning, T. H., Gaussian Basis Sets for Use in Correlated Molecular Calculations. I. The Atoms Boron through Neon and Hydrogen. *J. Chem. Phys.* **1989,** *90*, 1007-1023.
28. Ditchfield, R.; Hehre, W. J.; Pople, J. A., Self-Consistent Molecular-Orbital Methods. IX. An Extended Gaussian-Type Basis for Molecular-Orbital Studies of Organic Molecules. *J. Chem. Phys.* **1971,** *54*, 724-728.
29. Yanai, T.; Tew, D. P.; Handy, N. C., A New Hybrid Exchange–Correlation Functional using the Coulomb-Attenuating Method (CAM-B3LYP). *Chem. Phys. Lett.* **2004,** *393*, 51-57.
30. Slater, J. C.; Phillips, J. C., *Quantum Theory of Molecules and Solids, Vol. 4: The Self-Consistent Field for Molecules and Solids*. McGraw-Hill: New York: 1974; p 49.

31. Vosko, S. H.; Wilk, L.; Nusair, M., Accurate Spin-Dependent Electron Liquid Correlation Energies for Local Spin Density Calculations: A Critical Analysis. *Can. J. Phys.* **1980,** *58*, 1200-1211.
32. Becke, A. D., Density-Functional Exchange-Energy Approximation with Correct Asymptotic Behavior. *Phys. Rev. A* **1988,** *38*, 3098-3100.
33. Becke, A. D., Density-Functional Thermochemistry. III. The Role of Exact Exchange. *J. Chem. Phys.* **1993,** *98*, 5648-5652.
34. Lee, C.; Yang, W.; Parr, R. G., Development of the Colle-Salvetti Correlation-Energy Formula into a Functional of the Electron Density. *Phys. Rev. B* **1988,** *37*, 785-789.
35. Grimme, S.; Antony, J.; Ehrlich, S.; Krieg, H., A Consistent and Accurate *ab initio* Parametrization of Density Functional Dispersion Correction (DFT-D) for the 94 Elements H-Pu. *J. Chem. Phys.* **2010,** *132*, 154104.
36. Marten, B.; Kim, K.; Cortis, C.; Friesner, R. A.; Murphy, R. B.; Ringnalda, M. N.; Sitkoff, D.; Honig, B., New Model for Calculation of Solvation Free Energies: Correction of Self-Consistent Reaction Field Continuum Dielectric Theory for Short-Range Hydrogen-Bonding Effects. *J. Phys. Chem.* **1996,** *100*, 11775-11788.
37. Rashin, A. A.; Honig, B., Reevaluation of the Born Model of Ion Hydration. *J. Phys. Chem.* **1985,** *89*, 5588-5593.
38. Wang, H., An Accurate Theoretical Study of Energy Barriers of Alkaline Hydrolysis of Carboxylic Esters. *Res. Chem. Intermed.* **2012,** *38*, 2175-2190.
39. Li, C.; Zheng, X.; Su, N. Q.; Yang, W., Localized Orbital Scaling Correction for Systematic Elimination of Delocalization Error in Density Functional Approximations. *Natl. Sci. Rev.* **2017,** *5*, 203-215.
40. Su, N. Q.; Mahler, A.; Yang, W., Preserving Symmetry and Degeneracy in the Localized Orbital Scaling Correction Approach. *J. Phys. Chem. Lett.* **2020,** *11*, 1528-1535.
41. Mei, Y.; Yu, J.; Chen, Z.; Su, N. Q.; Yang, W., LibSC: Library for Scaling Correction Methods in Density Functional Theory. *J. Chem. Theory. Comput.* **2022,** *18*, 840-850.